NanoImpact 14 (2019) 100168

Contents lists available at ScienceDirect

NanoImpact

journal homepage: www.elsevier.com/locate/nanoimpact

Physicochemical alterations and toxicity of InP alloyed quantum dots aged in environmental conditions: A safer by design evaluation

Adeline Tarantini[a,1], K. David Wegner[b,1], Fanny Dussert[a], Géraldine Sarret[c], David Beal[a], Lucia Mattera[b], Christophe Lincheneau[b], Olivier Proux[d,e], Delphine Truffier-Boutry[f], Christine Moriscot[i], Benoit Gallet[g], P.-H. Jouneau[h], Peter Reiss[b], Marie Carrière[a,*]

[a] Univ. Grenoble Grenoble Alpes, CEA, CNRS, INAC-SyMMES, CIBEST, 38000 Grenoble, France
[b] Univ. Grenoble Grenoble Alpes, CEA, CNRS, INAC-SyMMES, STEP, 38000 Grenoble, France
[c] ISTerre (Institut des Sciences de la Terre), Univ. Grenoble Alpes, CNRS, IRD, IFFSTAR, Univ. Savoie Mont Blanc, 38000 Grenoble, France
[d] BM30B/FAME beamline, ESRF, 38043 Grenoble, France
[e] Observatoire des Sciences de l'Univers de Grenoble, 38000 Grenoble, France
[f] CEA-LITEN L2N, 17 rue des Martyrs, 38054 Grenoble Cedex 9, France
[g] CNRS, CEA, IBS, Grenoble, France
[h] Univ. Grenoble Grenoble Alpes, CEA, CNRS, INAC-MEM, LEMMA, 38000 Grenoble, France
[i] Integrated Structural Biology Grenoble (ISBG) CNRS, CEA, Univ. Grenoble-Alpes, EMBL, 71 rue des Martyrs, F-38042, Grenoble, France

ARTICLE INFO

Keywords:
Quantum dot
Semiconductor nanocrystal
Toxicity
Keratinocyte
EXAFS

ABSTRACT

Due to their unique optical properties, quantum dots (QDs) are used in a number of optoelectronic devices and are forecasted to be used in the near future for biomedical applications. The most popular QD composition consists of cadmium selenide (CdSe) or cadmium telluride (CdTe), which has been shown to pose health risks due to the release of toxic cadmium (Cd) ions. Due to similar optical properties but lower intrinsic toxicity, indium phosphide (InP) QDs have been proposed as a safer alternative. Nevertheless, investigations regarding their safety and possible toxicological effects are still in their infancy.

The fate and toxicity of seven different water-dispersible indium (In)-based QDs, either pristine or after ageing in a climatic chamber, was evaluated. The core of these QDs was composed of indium, zinc and phosphorus (InZnP) or indium, zinc, phosphorus and sulfur (InZnPS). They were assessed either as core-only or as core-shell QDs, for which the core was capped with a shell of zinc, selenium and sulfur (Zn(Se,S)). Their surface was functionalized using either penicillamine or glutathione.

In their pristine form, these QDs showed essentially no cytotoxicity. The particular case of InZnPS QD showed that core-shell QDs were less cytotoxic than core-only QDs. Moreover, surface functionalization with either penicillamine or glutathione did not appreciably influence cytotoxicity but affected QD stability. These QDs did not lead to over-accumulation of reactive oxygen species in exposed cells, or to any oxidative damage to cellular DNA. However, accelerated weathering in a climatic chamber led to QD precipitation and degradation, together with significant cytotoxic effects. Ageing led to dissociation of In—P and Zn—S bonds, and to complexation of In and Zn ions with carboxylate and/or phosphate moieties.

These results show that InZnP and InZnPS alloyed QDs are safer alternatives to CdSe QDs. They underline the

Abbreviations: BrdU, bromodeoxyuridine; DDT, 1-dodecanethiol; EDS, energy dispersive X-ray spectroscopy probe; ESRF, European Synchrotron Radiation Facility; GSH, Glutathione; H2-DCF-DA, 2′,7′-dichlorodihydrofluorescein diacetate; DHR123, dihydrorhodamine 123; HAADF, high angle annular dark field; IARC, International agency for research in cancer; LCF, linear combination fit; LDH, lactate dehydrogenase; MMS, methane methyl sulfonate; MPA, mercaptopropionic acid; NC, Semiconductor nanocrystal; ODE, 1-octadecene; PL, photoluminescence; QD, Quantum dot; QY, Quantum yield; ROS, Reactive oxygen species; SEM, scanning electron microscope; STEM, scanning-transmission electron microscopy; TCEP, tris(2-carboxyethyl) phosphine hydrochloride; TMAOH, tetramethylammonium hydroxide; $(TMS)_3P$, tris(trimethylsilyl)phosphine; TOP, trioctylphosphine; XAS, X-ray absorption spectroscopy

* Corresponding author at: INAC-SyMMES/CIBEST, 17 rue des Martyrs, 38000 Grenoble, France.
E-mail addresses: adeline.tarantini@cea.fr (A. Tarantini), Karl-david.wegner@cea.fr (K.D. Wegner), fanny.dussert@cea.fr (F. Dussert), geraldine.sarret@univ-grenoble-alpes.fr (G. Sarret), david.beal@cea.fr (D. Beal), lucia.mattera@cea.fr (L. Mattera), christophe.lincheneau@cea.fr (C. Lincheneau), proux@esrf.fr (O. Proux), delphine.boutry@cea.fr (D. Truffier-Boutry), christine.moriscot@ibs.fr (C. Moriscot), benoit.gallet@ibs.fr (B. Gallet), pierre-henri.jouneau@cea.fr (P.-H. Jouneau), peter.reiss@cea.fr (P. Reiss), marie.carriere@cea.fr (M. Carrière).
[1] These authors contributed equally to this work.

https://doi.org/10.1016/j.impact.2019.100168
Received 19 December 2018; Received in revised form 10 May 2019; Accepted 10 May 2019
Available online 12 May 2019

necessity to preserve as much as possible the structural integrity of QDs, for instance by developing more robust shells, in order to ensure their safety for future applications.

1. Introduction

Colloidal semiconductor nanocrystals, also termed quantum dots (QDs), possess unique optical properties including size-tunable absorbance and emission, narrow emission bands, high photoluminescence quantum yield (QY) and resistance to photobleaching (Alivisatos, 1996). This makes them attractive for a wide range of applications, such as biosensing and imaging (Wegner and Hildebrandt, 2015), in photovoltaics and light-emitting devices including light-emitting diodes, TVs and displays (Reiss et al., 2016). The most popular QD composition consist of II-VI QDs such as cadmium selenide (CdSe) and cadmium telluride (CdTe), which display the highest quantum yields and can be synthesized with a high degree of monodispersity (Wegner and Hildebrandt, 2015). However, these heavy metal containing QDs have been shown to be toxic in human and environmental models (Bottrill and Green, 2011; Rocha et al., 2017). The main reasons explaining their toxicity is the leakage of Cd ions during QD degradation, which results in the generation of reactive oxygen species (ROS) (Kauffer et al., 2014). QD degradation is triggered via surface oxidation by molecular oxygen from air and under UV irradiation, or in intracellular acidic compartments such as lysosomes (Corazzari et al., 2013; Derfus et al., 2004; Kirchner et al., 2005). Capping CdSe or CdTe cores with a shell of zinc sulfide (ZnS) not only improves their photophysical properties but also reduces their degradation and thus their toxicity (Bottrill and Green, 2011). However, cadmium (Cd) compounds are classified as carcinogenic to humans (Group 1) by the International Agency for Research on Cancer (IARC) (IARC, 1993), and their use in electrical and electronic equipment has been restricted in the European Union through the Restriction of Hazardous Substances (RoHS) directive (Directive 2011/65/EU of the European Parliament).

Recently, the concept of safer-by-design has been applied to nanoscience and nanotechnology with first reports published in the literature a little more than ten years ago (Schwarz-Plaschg et al., 2017). The core of this concept is the integration of safety considerations in the design of nanomaterials or nano-enabled products, to make sure that these products will have a low risk potential from their production until their end-of-life (Bastus and Puntes, 2018; Kraegeloh et al., 2018; Lin et al., 2018). In this context, a safer-by-design concept for QDs would include: i) replacement of potentially toxic elements like Cd by less toxic chemical elements, ii) enhancement of the structural stability limiting the release of chemical elements, and iii) prevention of toxic intermediates such as ROS during utilization.

In the literature, several alternative QD compositions have been proposed, which can be used to follow the safer-by-design concept of Cd-free QDs. Among them, the most promising candidates are III/IV and I/III/VI QDs based on indium (In), including indium phosphide (InP) and copper-indium-sulfur ($CuInS_2$) QDs (Reiss et al., 2016). Thereby, InP QDs are the first nanocrytals that made the transition from laboratory bench into a commercial application, namely in the generation of TV screens (Reiss et al., 2016). Their potential was further shown for medical applications, owing to their ability to quickly, efficiently and specifically target sentinel lymph nodes when subcutaneously injected in mice or rats, without causing overt toxicity (Helle et al., 2012; Lin et al., 2015; Pons et al., 2010; Yaghini et al., 2018; Yaghini et al., 2016). InP is classified as probably carcinogenic to humans by the IARC (IARC, 2006), and InP QDs have been shown to be toxic in some in vitro studies (Chibli et al., 2011; Soenen et al., 2014). Their toxicity was shown to be dependent on the cell line (Chibli et al., 2011), and to be correlated with ROS accumulation in exposed cells (Chibli et al., 2011; Soenen et al., 2014). Nevertheless, InP QDs are less toxic than CdSe QDs due to the lower toxicity of In ions released from QDs, compared to Cd ions (Brunetti et al., 2013). An advantage of InP QDs in comparison to Cd-based QDs is the covalent nature of the bond between In and phosphorous (P), which makes them more stable in comparison to the ionic bond of CdSe (Bharali et al., 2005). The passivation of the InP QDs with a semiconductor shell, such as ZnS or zinc selenide (ZnSe), improves their photoluminescence and their long-term stability as the core will be protected from oxidative degradation (Reiss et al., 2016). An important characteristic for a core/shell material is their lattice mismatch. The lattice mismatch for InP/ZnS is around 7%, but is only 3.3% for InP/ZnSe (Reiss et al., 2016). A gradient shell of a ZnSe rich layer close to the InP core, combined with a ZnS layer on the outside, have shown to result in improved photophysical properties and photostability (Lim et al., 2011). These more stable QDs would eventually be less toxic than InP/ZnS QDs. Finally, the quantum yield of InP QDs can be improved by alloying their core with zinc (Zn) and/or sulfur (S), leading to highly fluorescent indium-zinc-phosphorus (InZnP) or indium-zinc-phosphorus-sulfur InZnPS QDs (Huang et al., 2010; Ung et al., 2010). These QDs would have improved optical properties compared to InP/ZnS QDs, and consequently smaller quantities would be necessary to achieve the same brightness. Physical, chemical and toxicological properties of these emerging QDs have been well characterized in their pristine state. However, these QDs are intended to be integrated into electronic devices (Reiss et al., 2016), therefore they will be exposed to daylight under normal conditions of use and potentially at the end of their lifecycle if they are not properly recycled. Therefore, to take into account the whole life cycle of these products, their physicochemical transformation and toxicity should be also assessed after exposing them to UV light, in environmental conditions.

In accordance with these safer-by-design principles, we synthesized some In-based QDs with modified chemistry in order to minimize their hazard. QDs with a core composed of InZnP or InZnPS were prepared and further studied as core-only QDs or as core-shell QDs where the cores were capped with a gradient shell composed of zinc, sulfur and selenium (Zn(Se,S)). The intrinsic hydrophobic QDs were rendered water-soluble using a ligand exchange reaction with either D-penicillamine (Pen) or L-glutathione (GSH). Pen was chosen because the obtained QDs are very compact, which is beneficial in biosensing applications (Mattera et al., 2016), while GSH was chosen because it is a well-documented antioxidant (for review, see (Calabrese et al., 2017)), which would reduce the oxidative stress induced by the QDs, as reported by others (Chibli et al., 2011; Soenen et al., 2014). The toxicity of these In-based QDs was evaluated on primary keratinocytes isolated from skin explants from human donors, and compared to the toxicity of Cd-based QDs. These QDs were then weathered in environmental conditions, consisting of exposure to whole spectrum sunlight for 64 h, as suggested in the ISO norms 4892-1 (2000) and 4892-2 (2013) dedicated to accelerated weathering of plastic. This norm was chosen since QDs are aimed at being embedded in plastic matrixes before being incorporated in optoelectronic devices (Litvin et al., 2017). Toxicity of aged vs. pristine QDs was compared. Finally, the their transformation products of these QDs upon ageing were identified using extended X-ray absorption fine structure (EXAFS) spectroscopy.

2. Materials and methods

2.1. Chemicals and reagents

D-Penicillamine (Pen), L-glutathione reduced (GSH) > 98.0%, tetramethylammonium hydroxide (TMAOH), phosphate-buffered saline

solution (1xPBS), tris(2-carboxyethyl) phosphine hydrochloride solution 0.5 M (TCEP), indium acetate (99.99%), myristic acid (> 99%), tris(trimethylsilyl)phosphine (95%, $(TMS)_3P$), 1-octadecene (90%, ODE), 1-dodecanethiol (97%, DDT), trioctylphosphine (97%, TOP), sulfur (99.99%), selenium (99.99%), methanol, chloroform and hexane were purchased from Sigma-Aldrich. Zinc stearate (90%, $ZnSt_2$) was acquired from Riedel de Haen and oleic acid (70%) came from Fisher Chemicals. All chemicals were used as received without any further purification, unless stated otherwise. Cell culture medium and serum were purchased from Thermo Fisher Scientific. All other chemicals were purchased from Sigma-Aldrich and were > 99% pure. CdSe/ZnS QDs were purchased from Thermofisher Scientific (Qdot ITK carboxyl quantum dots).

2.2. QD synthesis and characterization

For preparation of indium-myristate, indium acetate (6.9 mmol), myristic acid (21.4 mmol) and ODE (15 mL) were mixed in a 50 mL three neck flask. The solution was stirred and degassed under vacuum for 3 h at 120 °C. After cooling to room temperature, the precipitated indium-myristate was washed with ca. 150 mL dry hexane before drying under vacuum and storing in the glove box. For preparation of zinc oleate (0.4 M), zinc acetate (5 mmol), 10 mmol oleic acid and 9.35 mL ODE were mixed in a 50 mL three neck flask. The mixture was heated under vacuum to 120 °C and stirred for 1 h to remove water and oxygen. Then the flask was backfilled with argon (Ar) and the solution was cooled down to room temperature. At around 70 °C, the solution was transferred to vial and flushed with Ar before storing it in a glove box. For a 0.4 M TOP-selenium (TOP-Se) stock solution, 2 mmol of selenium powder was dissolved in 5 mL trioctylphosphine (TOP) for 24 h. The preparation of a 0.4 M TOP-sulfur (TOP-S) stock solution was done similarly using elemental sulfur.

Then, InZnP and InZnPS QD cores were prepared as follows. For InZnP QDs, indium-myristate (0.1 mmol), $ZnSt_2$ (0.1 mmol) and 7.5 mL ODE were mixed in a 50 mL three-neck flask and degassed for 1 h. The flask was backfilled with Ar and the reaction mixture was rapidly heated to 300 °C in a molten salt bath. At ca. 100 °C 0.1 mmol $(TMS)_3P$ dissolved in 1 mL ODE was swiftly injected. After 20 min, the reaction was quenched by removing the salt bath and let cool down to room temperature. The QDs were purified by precipitating (1:1 v/v mixture of methanol/chloroform and acetone) and re-dispersing (chloroform) three times, and finally stored in hexane. The InZnPS core was prepared similarly including the addition of 0.1 mmol DDT in the initial reaction mixture.

Gradient shells were then grown on the surface of InZnP and InZnPS QD cores. After the synthesis of the cores, the solution was cooled down to 220 °C to stop the growth. 2.5 mL of the 0.4 M zinc-oleate (1 mmol) stock solution was added dropwise followed by the swift injection of 0.444 mL of TOP-Se (0.2 mmol) stock solution dissolved in 0.5 mL ODE and 1.57 mL of TOP-S (0.7 mmol) stock solution. The reaction mixture was heated to 300 °C using a heating mantle with a temperature rate of 10 °C per minute. The overall shell growth time was 20 min. The reaction was stopped by cooling down to room temperature. The same purification cycle was performed as described for the core synthesis.

2.3. Phase transfer

Both InP and CdSe (Qdot ITK carboxyl, Thermofisher) QDs were then transferred in aqueous solution, via phase transfer using either Pen or GSH. A 0.2 M solution of Pen was prepared by dissolving 30 mg of Pen in 1 mL of degassed MilliQ water. After addition of 200 μL of TCEP, the pH was adjusted to 9 with TMAOH (25 wt% in methanol) solution. The solution was degassed again, and 500 μL added to 1 mL of degassed colloidal solution of InP core or InP core/shell in chloroform with an approximate concentration of 3–5 μM. The biphasic mixture was stirred vigorously for 45 min at room temperature. The mixture was quickly centrifuged to obtain a clear phase separation. The upper layer containing the QDs in the aqueous phase was separated from the organic phase and purified from excess ligands using a NAP™10 size exclusion column (Sephadex™ G-25 DNA Grade from GE Healthcare). The column was equilibrated with PBS buffer, which was further used as eluent and storage buffer. The transferred QD samples were stored at 4 °C. For the phase transfer using GSH, 0.26 mM GSH was dissolved in 300 μL TMAOH and added to a 1 μM QD solution in chloroform. The solution was stirred overnight at room temperature. The phase-transferred QDs were extracted from the organic solution using 200 μL PBS buffer with 250 mM NaCl. After centrifugation at 4300 $\times g$ for 1 min, the organic layer was separated from the aqueous phase. In order to purify the QDs from the excess of ligands, they were precipitated with 300 mL ethanol and centrifugation for 1 min at 4300 $\times g$. The clear supernatant was discarded and the QDs redispersed with 200 μL 1× PBS buffer with 250 mM NaCl. This cycle was repeated three times before the final precipitate was redispersed in 1× PBS. The QDs were stored at 4 °C in the dark; they were table for at least one year.

2.4. Photophysical and structural characterization of InP QDs

Absorbance measurements were performed using Hewlett Packard 8452A spectrophotometer whereas the emission spectra were recorded using a Fluorolog FL3-22 spectrometer from Horiba-Jobin Yvon equipped with a 150 W xenon lamp for steady-state measurements and a NanoLED laser diode from Horiba with a wavelength of 350 nm and 1 MHz repetition for time-resolved measurements. Decay curves were fitted using Decay Analysis software from Horiba Scientist. Photoluminescence quantum yield measurements were performed at room temperature using an integration sphere, Hamamatsu Quantaurus Absolute PL quantum yield spectrometer or by relative fluorescence measurements using Fluorescein 27 in 0.1 M sodium hydroxide (NaOH) (QY = 93%) as standard. The hydrodynamic diameter of the water-dispersible InZnP and InZnPS QDs was measured by dynamic light scattering (Malvern Zeta Sizer NanoZS).

2.5. Electron microscopy

For pristine QD structural characterization, the elemental composition was analyzed using a Zeiss Ultra 55+ scanning electron microscope (SEM) equipped with an energy dispersive X-ray spectroscopy probe (EDS). Samples for EDS were prepared by drop-casting a concentrated dispersion of QDs on a cleaned silicon substrate.

For imaging and EDS analysis of QDs and aged QDs, a drop of QD suspension was deposited on copper grids coated with lacey carbon films, allowed to dry at room temperature, then by scanning-transmission electron microscopy (STEM) using a high angle annular dark field (HAADF) detector, on a FEI/Tecnai OSIRIS microscope operating at 200 kV. The chemical composition of regions of interest was then analyzed by EDS using the same microscope and configuration. For imaging of cells via transmission electron microscopy (TEM), after exposure to QDs, cells were rinsed with 0.1 M PHEM buffer (30 mM PIPES, 12.5 mM HEPES, 5 mM $MgCl_2$, 1 mM EGTA, pH 7), then fixed for 30 min at room temperature in 4% paraformaldehyde, 0.4% glutaraldehyde prepared in 0.2 M PHEM to which was added culture medium (V:V). They were then fixed for another 30 min at room temperature in 2% paraformaldehyde, 0.2% glutaraldehyde in 0.1 M PHEM. Cells were rinsed three times in 0.1 M PHEM and post-fixed in 1% osmium tetroxide (OsO4), 1.5% potassium ferrocyanide in 0.1 M PHEM buffer for 1 h at room temperature. After 3 washes in water, they were post-stained using 0.5% uranyl acetate in 30% ethanol for 30 min at room temperature, in the dark. Cells were then dehydrated in graded ethanol series, and embedded in Epon resin. Ultrathin sections were cut on a Leica UC7 ultra-microtome and collected on Formvar carbon coated copper grids. Images were recorded on a Tecnai G2 Spirit BioTwin (FEI) transmission electron microscope (TEM), operating at 120 kV, using an

ORIUS SC1000 CCD camera (Gatan). For EDS analysis, samples were carbon-coated, then imaged by STEM (HAADF) detector, on a FEI/Tecnai OSIRIS microscope operating at 200 kV. The chemical composition of regions of interest was then analyzed by EDS using the same microscope and configuration.

2.6. Weathering in the QSUN climatic chamber

Samples were exposed to UV lamps in a Q-SUN Xe-1 xenon arc test chamber (Q-LAB), providing full sunlight spectrum. Weathering conditions were adapted from the ISO norms 4892-1 (2000) and 4892-2 (2013), developed for studying the ageing of plastics. The irradiance and temperature were fixed at 1.44 W/m^2 (measured at 420 nm) and 40 °C, respectively, with no humidity control. QD suspensions were diluted in PBS at the final concentration of 1 µM (in 1 mL), deposited in rectangular standard quartz cuvettes (48 mm × 12.5 mm × 12.5 mm, pathlength 10 mm) closed with polytetrafluoroethylene (PTFE) stopper, then irradiated for 64 h under agitation.

2.7. Cell culture and exposure

Human skin samples were obtained following breast surgery from healthy female donors with their informed consent (Centre Hospitalier Universitaire de Grenoble, Grenoble, France). All experiments were performed in accordance with relevant guidelines and regulations. In particular, work was performed in agreement with article L1245-2 of the French Public Health Code on the use of surgical wastes for research purposes (https://www.legifrance.gouv.fr). All donors were Caucasian (20–40 years old), and their skin phototype was between I and II according to the Fitzpatrick classification scale (Fitzpatrick, 1988). Keratinocytes were isolated from these whole skin samples, as previously described (Mouret et al., 2006). They were grown in keratinocyte serum-free medium (KSF-M) supplemented with 1.5 ng/mL epidermal growth factor (EGF), 25 µg/mL bovine pituitary extract, 75 µg/mL primocin and then cultured at 37 °C in a humidified atmosphere containing 5% CO_2. For all experiments, cells were used at passages 1–3.

Cells were seeded in 96-well plates (cytotoxicity, proliferation and oxidative stress assays, 5000 cells per well), 24-well plates (comet assay, 62,500 cells per well), 4 chamber Labteks (electron microscopy, 35,000 cells per well) or 75 cm^2 flasks (X-ray absorption spectroscopy, 1.5 million cells per flask). When they reached 60% of confluence, they were exposed for 24 h to 6.25–200 nM (cytotoxicity and cell proliferation), 12.5–100 nM (oxidative stress) or 50 nM (comet assay, X-ray absorption spectroscopy, electron microscopy) of either pristine or aged QDs.

2.8. X-ray absorption spectroscopy

Pristine and aged QDs (1 µM and approximatively 10 µM, respectively), as well as keratinocytes exposed to 50 nM of pristine or aged QDs were analyzed by X-ray absorption spectroscopy (XAS). A drop of pristine or aged QDs was directly deposited on the sample holder. Regarding cell samples, they were rinsed twice with PBS, then harvested using trypsin, centrifuged and suspended in 10 mM HEPES buffer, pH 7.5, to which 10% of glycerol was added. This cell suspension was deposited on the dedicated sample holder. Both types of samples were immediately frozen by immersion in liquid nitrogen. Indium speciation was analyzed by In K-edge (27.94 keV) extended X-Ray absorption fine structure (EXAFS) spectroscopy on FAME (BM30B) beamline (Proux et al., 2005) at the European Synchrotron Radiation Facility (ESRF, Grenoble, France), operating in multi-bunch mode (150 to 200 mA). Spectra were recorded at 15–20 K using a liquid He cryostat. The beamline is equipped with a Si(220) monochromator (Proux et al., 2006). Spectra were recorded in fluorescence mode using a 30-element Ge detector. Three to seven spectra of 40 min each were averaged, depending on the signal. Data were normalized and treated using the Demeter software package (Ravel and Newville, 2005). Spectra for the pristine QDs were treated by shell fitting using ARTEMIS software (Ravel and Newville, 2005). In-O, In-P and In-S paths were calculated using FEFF code, based on the structure of In phosphate dehydrate (Sugiyama et al., 1999), InP and InS (Wyckoff, 1963), respectively. Spectra for the aged QDs and cells exposed to pristine and aged QDs were treated by linear combination fitting (LCF) using Demeter/ATHENA (Ravel and Newville, 2005) using the pristine QDs, In acetate and In phosphate as reference spectra.

In addition, aged QDs were studied by Zn K-edge EXAFS spectroscopy on the same beamline and in the same conditions and setup. EXAFS spectra were treated by LCFs using ZnS (bulk and nano), provided by M. Le Bars (Le Bars et al., 2018), several Zn phosphate minerals including hopeite ($Zn_3(PO_4)_2$, $4H_2O$), Zn phosphate dihydrate ($Zn_3(PO_4)_2$, $2H_2O$) and Zn-reacted hydroxylapatite containing 500 µg g^{-1} Zn prepared at pH 6, described in Panfili et al. (2005), Zn-GSH (10 mM Zn, 100 mM GSH, pH 4.5), and Zn complexed to malate in solution as proxy for Zn-carboxylate (Zn-COOH) complexes. All the standard spectra were recorded at 15 K except Zn phosphate dihydrate and Zn-reacted hydroxylapatite which were recorded at room temperature. The temperature has a great influence on the amplitude of ZnS spectrum (Gilbert et al., 2004), much less on more disordered phases like Zn phosphate, as shown for hopeite in Fig. S1. For the two spectra recorded at room temperature, an amplitude factor of 1.15 was used to correct for the temperature effect, based on hopeite data (Fig. S1).

2.9. Toxicity assessment

Cytotoxicity and cell proliferation were assessed on the same 96-well plate seeded with keratinocytes, exposed to QDs for 24 h. Exposure medium was sampled for lactate dehydrogenase (LDH) quantification, and bromodeoxyuridine (BrdU) assay was performed on cells. In these assays, triton X100 (1%) was used as positive control. Released LDH was quantified using LDH assay (Sigma-Aldrich), following the manufacturer's instructions. Briefly, 50 µL of each exposure medium was deposited on a clean 96-well plate, then 100 µL of LDH assay solution (LDH assay substrate/cofactor/dye, V:V:V) was added to each well, and incubated for 30 min at room temperature, in the dark. Assay reaction was stopped by adding 10 µl of hydrochloric acid (HCl) 1 N to each well, then absorbance at 490 nm was measured using a Spectramax M2 spectrofluorimeter (Molecular Device) and corrected by subtraction of absorbance at 690 nm. Cell proliferation was quantified using 5-Bromo-2′-deoxy-uridine (BrdU) assay (Roche), using manufacturer's instructions. After exposure to QDs and removal of exposure medium, 100 µL of the BrdU solution, diluted to the tenth in cell culture medium, was added in each well and incubated for 2 h at 37 °C. This labeling medium was then removed, and cells were rinsed and incubated with Fix/denat solution for 30 min, then with an anti-BrdU-peroxidase antibody diluted to the hundredth in antibody dilution solution. After incubation for 45 min at room temperature, cells were rinsed three times with PBS, 100 µL of substrate solution was added to each well and incubated for 30 min at room temperature, in the dark. Absorbance at 370 nm was then measured using a Spectramax M2 spectrofluorimeter (Molecular Device) and corrected by subtraction of absorbance at 492 nm. The whole experiment was repeated three to five times independently, on keratinocytes from different donors, with $n = 3$ in each independent experiment. Independently of these two experiments, cytotoxicity was evaluated by measuring cell metabolic activity, using WST-1 assay (Roche). Cells were exposed for 24 h to 100 µL of QDs, then QDs were removed and 100 µL of WST-1 as added to each well. After 45 min of incubation at 37 °C, absorbance at 450 nm was measured using a Spectramax M2 spectrofluorimeter (Molecular Device) and corrected by subtraction of absorbance at 650 nm.

Reactive oxygen species were quantified using H2-DCF-DA and dihydrorhodamine 123 (DHR123) reagents (Thermo-Fisher Scientific).

Cell culture medium was removed and 100 µL of a 25 µM H2-DCF-DA or of a 1 µM DHR123 solution was added to each well. After 40 min of incubation at 37 °C in the CO_2 incubator, the H2-DCF-DA (or DHR123) solution was replaced by QD suspensions. Fluorescence (λexc/λem 480/530 nm) was recorded immediately after exposing cells to QDs, then after 2 h, 4 h and 24 h of exposure. *Tert*-butyl-hydroperoxide (100 µM) was used as positive control for H2-DCF-DA assay, and H_2O_2 (500 µM) or $KBrO_3$ (1 mM) were used as positive control for DHR123 assay. The whole H2-DCF-DA experiment was repeated twice independently, on keratinocytes from different donors, with n = 3 in each independent experiment. For DHR123, the experiment was repeated twice on keratinocytes from the same donor, with $n = 3$.

Oxidative damage to DNA was assessed using comet and comet-Fpg assays, which probe strand breaks and alkali-labile sites, and Fpg-sensitive sites including oxidized purines such as 8-oxo-dGuo, respectively, as previously described (Armand et al., 2016). As positive control for alkaline comet assay, cells were exposed to 100 µM of methane methyl sulfonate (MMS) for 24 h. As positive control for Fpg-modified comet assays cells were exposed to 1 µM of riboflavin for 20 min, followed by irradiation with UVA (10 J/cm^2). Comets were scored using image analysis Comet IV software (Perceptive Instruments, Suffolk, UK), and median % DNA in tail was calculated for at least 50 comets per slide. Net Fpg sensitive sites (Net Fpg) were calculated as the difference in % DNA in tail between samples with Fpg incubation and samples with buffer incubation ((% DNA in tail from alkaline assay) – (% DNA in tail from Fpg-modified assay)). The whole experiment was repeated three to five times independently, on keratinocytes from different donors (n = 3–5).

3. Results

3.1. Synthesis and characterization of the Cd-free quantum dots

In the present study, the long-term stability and toxicity of two types of alloyed InP-based QDs were investigated. Thereby, InP QDs with a core composition of InZnP and InZnPS, passivated by the popular gradient shell composed of Zn(Se,S), was the center of the investigation (Lim et al., 2011). Similarly to CdSe and CdTe QDs (Bottrill and Green, 2011), capping InP cores with a shell of zinc sulfide (ZnS) improves their photophysical properties and reduces their degradation (Lim et al., 2011). Using similar one-pot synthesis method, it was previously shown that addition of sulfur during the core reaction results in InP QDs coated with a thin layer of ZnS. The presence of this layer of ZnS further enhances the photophysical properties and potentially facilitates the phase transfer (Li and Reiss, 2008). But the consequences of this thin ZnS layer on the growth of the gradient shell and for the structural and photophysical properties -and eventually for the cytotoxic potential- of the QDs is currently unknown. Therefore, core only and core/shell systems were prepared and studied.

The photophysical characterization of the two types of InP QD cores (InZnP and InZnPS) are shown in Fig. 1A. The presence of the sulfur precursor during the core synthesis is leading to blue shift of the absorbance and photoluminescence (PL) maximum as well as a linewidth narrowing from 79 nm to 61 nm for the PL of the InZnP and InZnPS

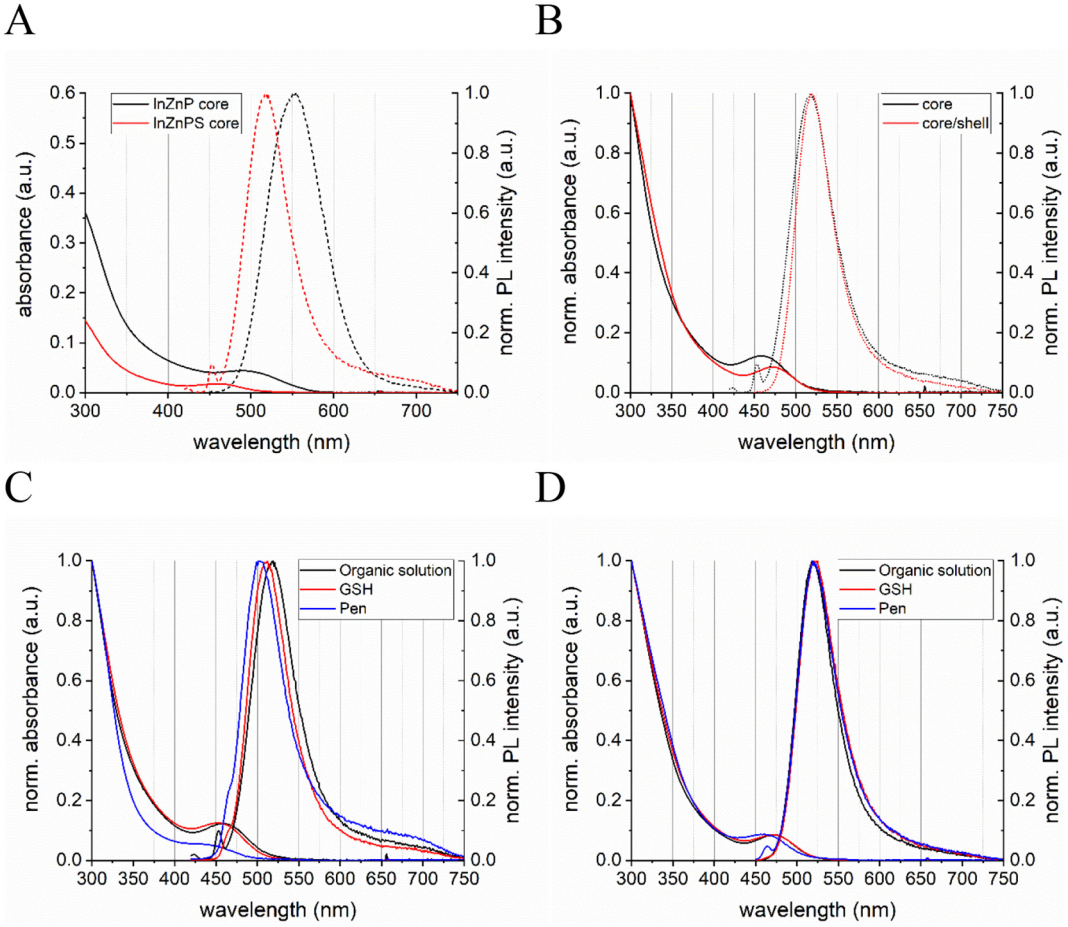

Fig. 1. Photophysical properties of InZnP and InZnPS QDs. Absorbance and normalized PL spectra of InZnP and InZnPS core QDs (A). Comparison of the normalized absorbance and PL spectra of InZnPS core and InZnPS QDs with a gradient shell of Zn(Se,S) (B). Comparison of the normalized absorbance and PL spectra of the InZnPS core (C) and InZnPS core/shell QDs (D) before the aqueous phase transfer (organic solution, black) and after using the ligands L-glutathione (GSH, red) and D-Penicillamine (Pen, blue).

core, respectively (Table S1). However, the InZnP core shows, with 15%, a nearly twice as high QY in comparison to the core prepared in presence of the sulfur precursor. After the epitaxial growth of the gradient Zn(Se,S) shell on the InZnPS core, the absorbance of the 1st excitonic peak shows a redshift of 12 nm whereas the PL maximum did not change (see Fig. 1B and Table S2). The shell growth has a stronger influence on the photophysical properties for the InZnP core as the 1st excitonic peak shows a redshift of 40 nm and the PL maximum is shifted by 17 nm (Fig. S2 and Table S3). These photophysical differences between both cores indicates that the Zn(Se,S) shell thickness is lower in the case of InZnPS (Tamang et al., 2016).

To use either the core or the core/shell QDs for the envisaged toxicological evaluations, they needed to be made water-dispersible. Strong differences between those two core materials could be observed during the phase transfer from the organic solution to aqueous solution using either D-penicillamine (Pen) or L-glutathione (GSH) as hydrophilic surface ligands. Whereas the InZnPS core material can be transferred using both ligands, InZnP core could not be transferred using Pen, because the core disintegrated during the process. As shown in Fig. 1C, the phase transfer led to a slight blue shift of the InZnPS core for the absorbance and PL maxima, which could in principle indicate a slight size reduction due to the removal of surface atoms. Interestingly, using GSH for the phase transfer of InZnP cores led to a PL redshift of around 42 nm with no change in the 1st excitonic maxima (Fig. S3 and Table S4). Spectral shifts are also observed for the core/shell systems as a function of their composition and phase transfer ligand used (see below). We attribute these shifts to contributions from the quantum confined Stark effect and solvatochromatic effects experienced by the QDs when changing their dielectric surrounding composed of the surface ligands and the solvent (Thuy et al., 2007). For both core materials, the PL QY dropped dramatically below 1% after the transfer. After the shell growth both core types could be transferred to aqueous solution either using Pen or GSH. The InZnPS core with the gradient Zn(Se,S) shell showed only small changes in the absorbance and PL maxima when transferred using GSH or Pen (Fig. 1D and Table S5) whereas the InZnP-based core/shell QDs exhibited a 22 nm blue shift of the excitonic peak when using Pen, a 6 nm shift with GSH (see Fig. S4 and Table S6).

The samples were further analyzed regarding their structural properties. After the phase transfer using different surface ligands, we investigated the influence on their hydrodynamic radius. As shown in Fig. S5 and in Table S7 and S8, a marked size difference of around 2 nm is observed between the alloyed InZnP core and core/shell QDs corresponding to a gradient shell thickness of approximately 3 monolayers. The size difference between the core and core/shell QDs is smaller in the case of InZnPS (around 0.7 nm), in accordance with a shell thickness of one monolayer.

3.2. Toxicity of alloyed InP QDs

Due to their photophysical properties, InP QDs would possibly interfere with classically-used toxicity assays. Therefore, optical interference was assessed by measuring absorbance emission at the wavelengths that are typically used in toxicity assays (Fig. S6). The lowest interference was found at the wavelength used in LDH assay. Chemical interference of QDs with the chemical reactions taking place in LDH assay was then assessed; it was shown to be minor (Table S9). Therefore, LDH assay was chosen for cytotoxicity assessment. Following our initial hypotheses, we compared the toxicity of core-only vs. core-shell QDs, with a core composed of InZnPS vs. a core composed of

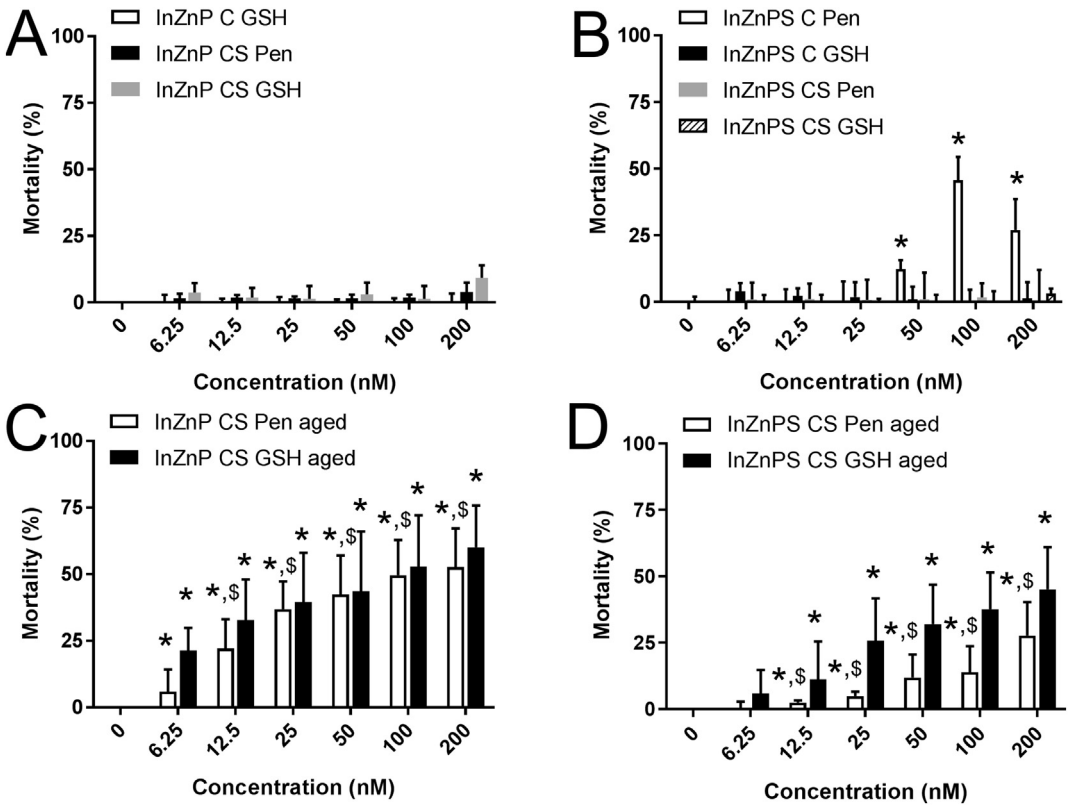

Fig. 2. Cytotoxicity of InZnP and InZnPS QDs, assessed via the lactate dehydrogenase assay. Cells were exposed to pristine QDs (A-B) or QDs exposed to simulated sunlight (aged, C-D), with a core of InZnP (A, C) or InZnPS (B, D). C: core only, CS: core-shell structure; Pen, GSH: penicillamine or glutathione, respectively, was used as surface ligand. Triton X-100 (1%) was used as positive control. Results are expressed as % relative to the control (unexposed cells). Graphs represent mean ± standard deviation of 3 to 6 independent experiments, performed on keratinocytes from different donors, with 3 replicates per experiment, statistical significance: $p < 0.05$, *: exposed vs. control, $: InZnP vs. InZnPS.

InZnP, and coated with Pen vs. coated with GSH (Fig. 2A-B). Among the core-only QDs, since InZnP QD could not be transferred to aqueous phase in Pen, we compared the toxicity of InZnP with GSH as surface ligand to that of InZnPS with either GSH or Pen as surface ligand. Only the core-only QD with a core composed of InZnPS and with Pen as surface ligand significantly altered cell viability. None of the other core-only QDs, and none of the tested core-shell QDs showed significant cytotoxicity in their pristine state. WST-1 assay, which measures cell metabolic activity and is also classically used to assess cytotoxicity confirmed these results (Fig. 3). For comparison, exposure to 100 nM or 200 nM of pristine CdSe/ZnS QDs caused the mortality of 27% and 41% of the cells, respectively (Fig. S7).

Then, toxicity of these QDs was assessed after ageing for 64 h in a climatic chamber. After exposure to simulated sunlight, all core-shell QDs showed significant cytotoxicity (Fig. 2C-D). Comparing the core-shell QDs with respect to their core composition, cells exposed to aged InZnPS-based QDs showed a lower mortality rate than cells exposed to QDs with InZnP core. No significant differences was observed between QDs coated with either Pen or GSH. (Fig. 2C-D). The toxicity of aged CdSe QDs was similar, with 36 to 66% of mortality in cells exposed to 12.5 to 200 nM of aged CdSe QDs (Fig. S7).

Although they did not induce any cytotoxicity, all pristine QDs significantly decreased cell proliferation, with no significant difference between pristine QDs with a core of InZnP or InZnPS, or with Pen or GSH as surface ligand (Fig. 4A-B). Decreased cell proliferation results from cell cycle arrest. Since one of the causes of cell cycle arrest is DNA alteration, the impact of pristine QDs on DNA integrity was evaluated. The occurrence of DNA strand breaks, alkali-labile sites and Fpg-sensitive sites such as 8-oxo-dGuo was explored using the Comet assay, in its alkaline and Fpg-modified versions. The investigation using core-only and core-shell InZnPS QDs coated with Pen revealed no DNA strand-breaks and/or alkali-labile sites (Fig. 4C). Neither did they increase the level of oxidized purines (Fig. 4D) and the intracellular level of reactive oxygen species, as assessed via 2′,7′-dichlorodihydrofluorescein diacetate (H2-DCF-DA) (Fig. 4E-F for times 0 to 24 h and Fig. S8 for times 0 to 4 h of exposure) and via dihydrorhodamine 123 (DHR123) (Fig. S9) assays. Interference of QDs with these two assays was assessed, it was significant for some QDs in DHR123 assay, but only minor interference was found with H2-DCF-DA (Table S10).

3.3. Physicochemical transformation of In-based QDs after accelerated weathering in a climatic chamber

Since QDs exposed to simulated sunlight were much more toxic than pristine QDs, their physical and chemical transformation upon irradiation was characterized. Visual observation showed a gradual precipitation of the QD suspension, which was still fluorescent, followed by a progressive loss of the fluorescence leading finally to a red-purple transformation product. When imaged by TEM, pristine QDs appeared as nanoparticles with 3–5 nm diameter (Fig. 5A), while aged QDs appeared as large precipitates with heterogeneous structure (Fig. 5B-C). Some areas in these precipitates were composed of In, P, Zn, O and S, while Se and S precipitated separately, as probed by EDS analysis (Fig. 5D-I).

Irradiation with simulated sunlight resulted in a marked changed in In speciation, as assessed by EXAFS at the In K-edge. In pristine QDs, In was mainly bound to P atoms, with a main peak of the Fourier transformed spectra at $R + \Delta R = 2$ Å (Fig. 6A-B). The local structure differed slightly from the structure of bulk indium phosphide, in which In is bound to 4 atoms of P at 2.54 Å (Wyckoff, 1963). A minor contribution of O and S was found for the InZnP and InZnPS core-shell QDs, respectively (Table 1). The presence of S in the In coordination shell is consistent with previous observations on InZnPS QDs, and is due to the presence of a mixed layer at the core-shell boundary (Cho et al., 2016). The presence of O may arise from the persistence of a minor amount of In precursor after purification in this particular sample. When analyzing aged QDs, whatever their initial composition, the first peak of the Fourier-transformed spectra was at $R + \Delta R = 1.65$ Å. This is consistent with coordination of In with O-containing ligands (Fig. 6C-D). Regarding Zn, a drastic change in speciation was also observed. For pristine QDs, the main peak of the Fourier transformed spectrum was at $R + \Delta R = 1.95$ Å (Fig. 7), suggesting that Zn was bound to S and possibly Se and P atoms. For aged QDs, the position of the main peak was characteristic of O ligands, and spectra were reproduced by 100% Zn phosphate compounds (the proportions of each species are given in the legend of Fig. 7). The In and Zn EXAFS data suggest complete dissolution of QDs during ageing, the binding of In to COOH and phosphate moieties, and of Zn to phosphate moieties. Pen and CO_2 from air were the only conveyer of –COOH moieties, while phosphate was present in the buffer (PBS) in which QDs were initially dispersed.

3.4. Intracellular distribution

Intracellular accumulation of pristine QDs could not be identified via TEM, because these QDs were too small to be distinguished from cytoplasmic components. Therefore, cells exposed to pristine QDs looked like control cells, with a typical morphology of human primary keratinocytes (Fig. 8A). Conversely, electron-dense precipitates were

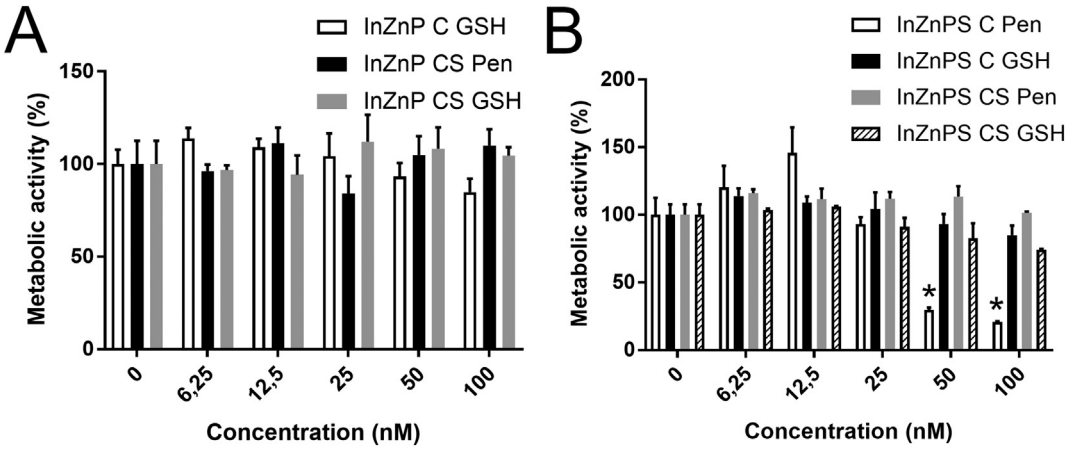

Fig. 3. Cytotoxicity of InZnP and InZnPS QDs, assessed via the WST-1. Cells were exposed to pristine QDs with a core of InZnP (A) or InZnPS (B). C: core only, CS: core-shell structure, Pen, GSH: penicillamine or glutathione, respectively, was used as surface ligand. Triton X-100 (1%) was used as positive control. Results are expressed as % relative to the control (unexposed cells). Graphs represent mean ± standard deviation of 2 independent experiments, performed on keratinocytes from the same donor, with 3 replicates per experiment, statistical significance: $p < 0.05$, *: exposed vs. control.

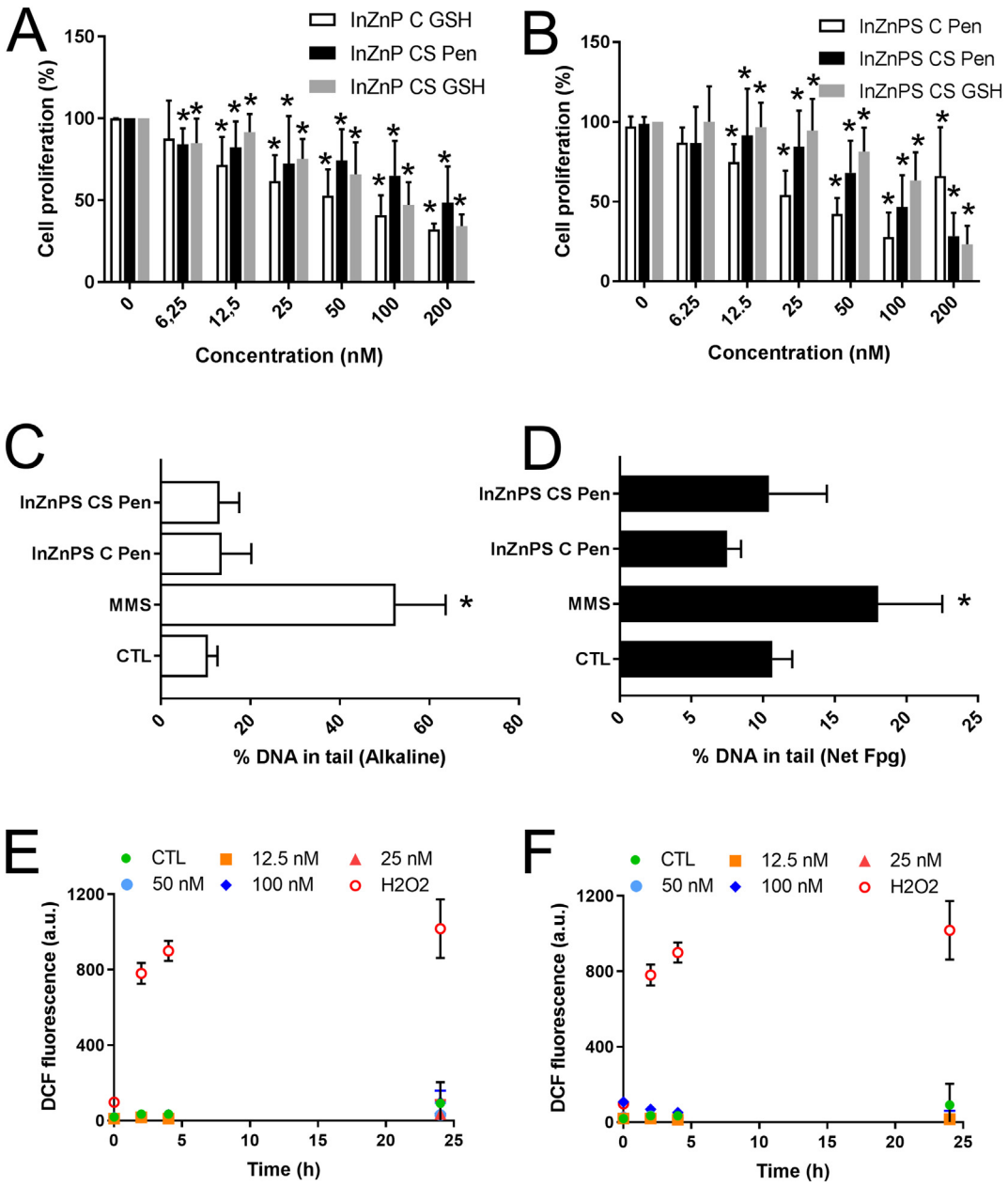

Fig. 4. Impact of sub-lethal concentrations of pristine QDs on cell proliferation, DNA integrity and intracellular level of reactive oxygen species. BrdU proliferation assay on cells were exposed to pristine QDs with a core of InZnP (A) or InZnPS (B). DNA integrity assessed via comet assay, in the alkaline version (C) or the Fpg-modified version (D). Intracellular level of reactive oxygen species assessed via DCFH-DA assay, on keratinocytes exposed to InZnP CS Pen (E) or InZnPS CS Pen (F). C: core only, CS: core-shell structure, Pen: penicillamine was used as surface ligand, GSH: glutathione was used as surface ligand. Tert-butyl hydroperoxyde (H_2O_2), 100 µM, was used as positive control. Graphs represent mean ± standard deviation of 3 to 5 independent experiments, performed on keratinocytes from different donors, with 3 replicates per experiment ($n = 3$), except for E and F where graphs represent mean ± standard deviation of a single experiment with 5 independent replicates ($n = 5$). Statistical significance *p < 0.05, exposed vs. control.

observed in the cytoplasm of cells exposed to aged QDs, sometimes as large as 5 µm (Fig. 8B, stars). No clear confinement in cytoplasmic vesicles surrounded by a membrane could be identified. These precipitates were not observed in the cell nucleus nor in mitochondria or any other organelles, but they were often observed close to the nuclear membrane. STEM observation (Fig. 8C), coupled to EDS analysis (Fig. 8D-E) of one of these electron-dense regions revealed that it contained In, P, Zn, Se and S, and that In co-precipitated with P, Zn and O while Se and S co-precipitated independently.

In cells exposed to pristine QDs In speciation did not change further, except in cells exposed to the core-only InZnP QD coated with GSH. Under this condition, a partial dissolution was observed with the formation of In-COOH and In-phosphate species (Fig. 6C-D, Table 2). In cells exposed to aged QDs, In speciation was unchanged, considering an uncertainty of ± 10% on the percentages.

4. Discussion

We explored the potential of alloyed InP QDs as safer alternatives to Cd-based QDs, using a safer-by-design strategy which combined i) replacement of Cd by In, ii) covering of InP core with a gradient shell composed of Zn(Se,S), iii) alloying of the InP core with either Zn or Zn and S, in order to improve their optical properties and their chemical stability. The main result of this work is that the cytotoxicity of pristine

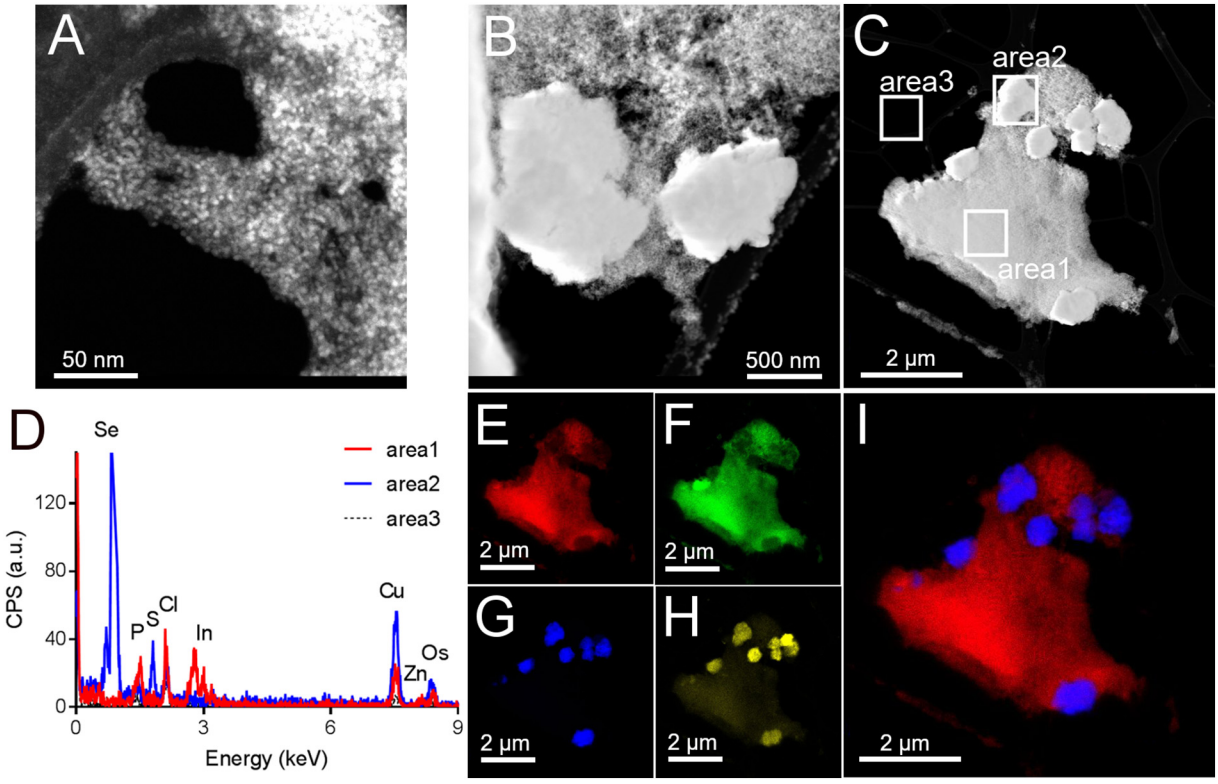

Fig. 5. TEM and STEM imaging, EDS analysis of pristine and aged core-shell InZnPS/Zn(Se,S) QDs. Pristine (A) and aged (B) QDs were imaged by TEM, then aged QDs were imaged by STEM (C) and analyzed by EDS (D-I). D: EDS spectra of areas 1, 2 and 3 as highlighted in C. Reconstruction of the distribution of In (E), P (F), Se (G), S (H); distribution of both In and Se (I).

QDs used in this study, regardless of their composition and structure, is lower than the cytotoxicity of CdSe/ZnS QDs. It is also lower than the cytotoxicity reported by others for InP/ZnS QDs, in vivo and in vitro (Lin et al., 2015; Yaghini et al., 2018; Yaghini et al., 2016; Chibli et al., 2011; Soenen et al., 2014; Brunetti et al., 2013). Conversely all aged QDs show some cytotoxicity. It is important to note that, in their pristine form, both core-only and core-shell QDs are very stable in exposure medium when coated with Pen or GSH. They show no significant agglomeration, whereas aged QDs agglomerate and would consequently immediately settle and interact with cell monolayers for longer periods of time. This would drastically change the effective exposure concentration, which is certainly much higher for cells exposed to aged QDs than for pristine QDs. Consequently, toxicity of pristine vs. aged QDs cannot be directly compared and are discussed separately.

Among pristine QDs, only InZnPS-C-Pen shows cytotoxicity. Conversely, InZnPS-C-GSH (i.e., the QD with the same core composition but different surface coating) and InZnPS-CS-Pen (its core-shell counterpart) are not cytotoxic. This suggests that the presence of a shell reduces the toxicity of this QD, and that surface functionalization does not appreciably influence the cytotoxicity. Noteworthy, ligand exchange of core-only InZnP QDs using Pen is not possible, because these QDs readily degrade during this process. Conversely, core-only InZnPS QDs, in which alloying the core with S results in the formation of a thin, protective layer of ZnS on top of the core (Li and Reiss, 2008), can be transferred with Pen without degrading, i.e. are more chemically stable. Both core-only InZnP and InZnPS can be transferred using GSH, which result in stable and non-cytotoxic suspensions. This suggests that using GSH for ligand exchange leads to a better stabilization of the QD core than Pen, at least in the case of core-only QDs. This behavior can be explained by the chemical nature of GSH, which is, compared to Pen, a more complex molecule containing one amino and two carboxy-groups. The bigger size and different structure with a potential better binding towards the QD surface will support QD integrity during the ligand exchange and afterwards. Regarding core-shell QDs, they can be transferred using both Pen and GSH, and are all stable and non-cytotoxic. Therefore, coating InZnP and InZnPS core with a layer of Zn(Se,S) prevents their degradation, similar to coating CdSe and InP QDs with a shell of ZnS, which protects them from degradation (Chibli et al., 2011; Lim et al., 2011).

Conversely, ageing leads to a drastic chemical transformation of these QDs, including loss of the structure of QD core and Zn(Se,S) gradient shell This leads to the precipitation of In(III) and Zn(II) with phosphate and carboxylate moieties which are provided, respectively, by the PBS buffer and by Pen and dissolution of CO_2 from air in the aged QD suspension. Although the speciation of Se has not been studied here, EDS analysis shows that Se and S co-precipitate, and the red-purple color of QD precipitate which is observed after 64 h of ageing certainly originates from this co-precipitation. Oxidative degradation of CdSe/ZnS core/shell QDs has been largely documented. It relies on chemical oxidation of Se and S from the surface of QDs, which first produces lattice structural defects, then leads to the release of soluble and toxic Cd, Se, Zn and S ions (Mancini et al., 2008). Our hypothesis is that the degradation of InP QDs follows the same stages. The gradual degradation of the InZnP and InZnPS structures based on the oxidation of core and shell elements can be monitored by the fluorescence quenching and the subsequent release of In(III) and Zn(II) ions, complexing quickly with available oxygen-rich ligands, i.e. phosphates and carboxylates.

All aged QDs significantly affect cell viability. The degradation products of these QDs (such as In-phosphate and/or –carboxylate, Zn-phosphate and selenium sulfur co-precipitates for core-shell QDs) accumulate in cells and may explain their toxicity. The toxicity of indium, either as In ions or as In-containing particles, has been rarely reported. It has been shown to depend on the cell type (Huaux et al., 2018). Moreover, several studies suggest that it may depend on In speciation, particularly on the potential of In-containing particles to dissolve and

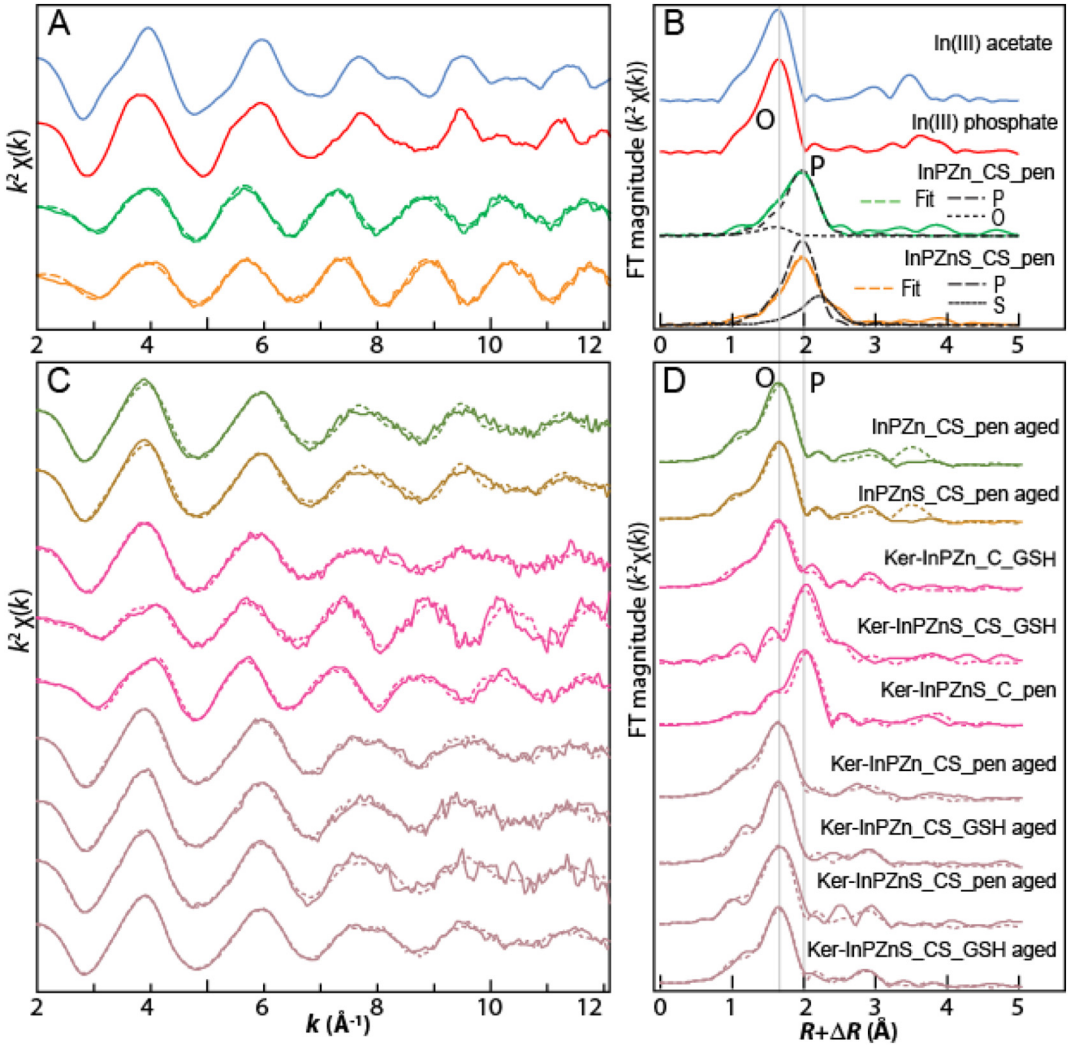

Fig. 6. EXAFS analysis of QDs and keratinocytes exposed to QDs, at the In K-edge. Analysis by shell fitting of pristine QDs with InZnP and InZnPS core and Zn(Se,S) shell, coated with Pen (structural parameters are presented in Table 1), and comparison of the spectra with two reference compounds having O as first neighboring atom (A-B). Analysis by linear combination fitting of aged QDs and keratinocytes exposed to pristine and aged QDs (LCF results are presented in Table 2) (C-D). Data are presented as k^2-weighted EXAFS spectra (A, C) and Fourier transforms (B, D).

Table 1
First shell structural parameters for the pristine QDs obtained by shell fittings of the EXAFS spectra, at the In K-edge[a].

	Atom	R (Å)	N	σ^2(Å^2)	R factor
InZnP-CS-Pen	O	2.15	0.6	0.0022	0.016
	P	2.49	3.4	0.0022	
InZnPS-CS-Pen	P	2.47	3.1	0.0010	0.011
	S	2.74	0.9	0.0010	

[a] *N*: number of atoms, *R*: interatomic distance, σ^2: Debye-Waller factor, *R factor*: residual between fit and experiment. Fits performed in the *k* range [2.3–13.5 Å^{-1}], and *R* range [0.8–2.7 Å].

release In ions. For instance, $InCl_3$ is not cytotoxic, but it has been shown to be genotoxic via the generation of ROS (Lin et al., 2013). Indium-tin-oxide NPs (ITO), consisting of 90% In_2O_3 and 10% SnO, are cyto- and genotoxic at high concentration, and these effects are correlated with oxidative stress and release of In ions from particles (Bomhard, 2016). Accordingly, InP was shown to be significantly more toxic than ITO, due to the higher solubilization and release of In ions from InP, compared to ITO (Bomhard, 2016; Gwinn et al., 2015). The cellular impacts of zinc are well documented. Zn is an essential trace element, which is crucial for the structure and function of many proteins, and thereby is necessary for a plethora of cellular functions (Jarosz et al., 2017; Sharif et al., 2012). It has been shown to alleviate the cellular toxicity of a number of toxicants, including non-essential metals, mainly because it activates the expression of metallothioneins and acts as an antioxidant (Rahman et al., 2019). Its antioxidant potency relies primarily on activation of some antioxidant proteins such as superoxide dismutase and catalase, on replacement of oxidant metals such as iron and copper in some metal-binding sites in cells and on antagonizing transition-metal catalyzed reactions (Jarosz et al., 2017). Nevertheless, at higher doses Zn provided as Zn(II) ion or as Zn-containing NPs such as ZnO-NPs, is cytotoxic (Beyersmann and Haase, 2001; Vandebriel and De Jong, 2012). In skin cells, ZnO-NPs cause mitochondrial dysfunction and ROS production, p53 pathway activation, cell cycle perturbation and eventually apoptosis (Vandebriel and De Jong, 2012). Therefore, the release of In(III) and Zn(II) during the degradation of QDs may explain the cytotoxicity of aged QDs. It may also explain why pristine QDs, which are chemically more stable, show essentially no cytotoxicity. However, the behavior of two pristine QDs does not conform to this hypothesis. InZnPS core QD coated with Pen shows significant cytotoxicity, while EXAFS analysis shows no major change in In speciation, i.e. no major degradation of this QD. One hypothesis could be that low-grade degradation occurs, via interaction of QDs or their surface ligand with intracellular components, which would

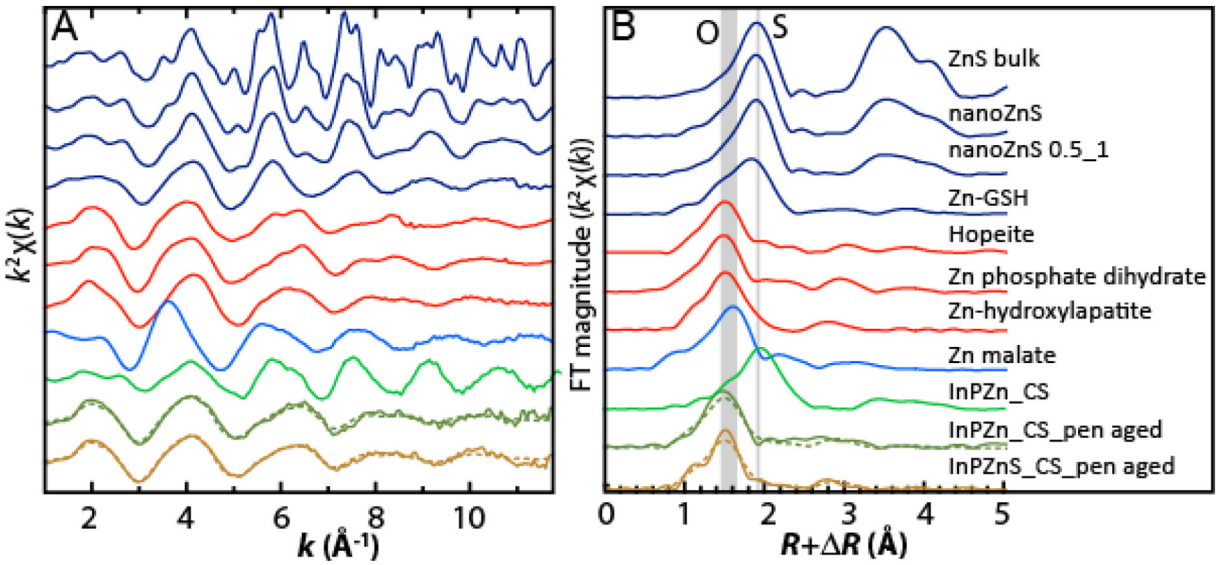

Fig. 7. EXAFS analysis of QDs at the Zn K-edge. EXAFS spectra (A) and Fourier transforms (B) for Zn reference compounds, pristine and aged QDs. Peak positions characteristic of O and S neighboring atoms are indicated by grey lines in B. Spectra for aged InZnP and InZnPS QDs were both reproduced by a combination of 50% Zn phosphate dihydrate and 50% Zn-hydroxyapatite (dashed lines in A and B, with R-factors, residual between fit and experiment of 0.07 and 0.04, respectively).

lead to the release of a small amount of toxic ions from QDs, as already suggested by Soenen et al. (Soenen et al., 2014). This small amount would be sufficient to cause cell death but would not be detected by EXAFS (the limit of detection of a specific chemical species using this technique is 10%). Low-grade degradation, not-observed via EXAFS, would also explain the cell cycle disturbance, leading to decreased proliferation of cells exposed to pristine QDs. Moreover, InZnP core-only QD coated with GSH are not stable, i.e. EXAFS analysis shows that it degrades inside cells, while it is not cytotoxic. This could suggest that In(III) and Zn(II) are scavenged by GSH, due to the high affinity for metals of its thiol group.

Finally, although InP/ZnS QDs have been shown to generate ROS ex cellulo (Chibli et al., 2011) and their toxicity has been related to oxidative stress (Soenen et al., 2014), InZnPS QDs, both core-only and core-shell and coated with Pen do not induce any oxidative stress. This divergence could be explained by the different QDs used in those

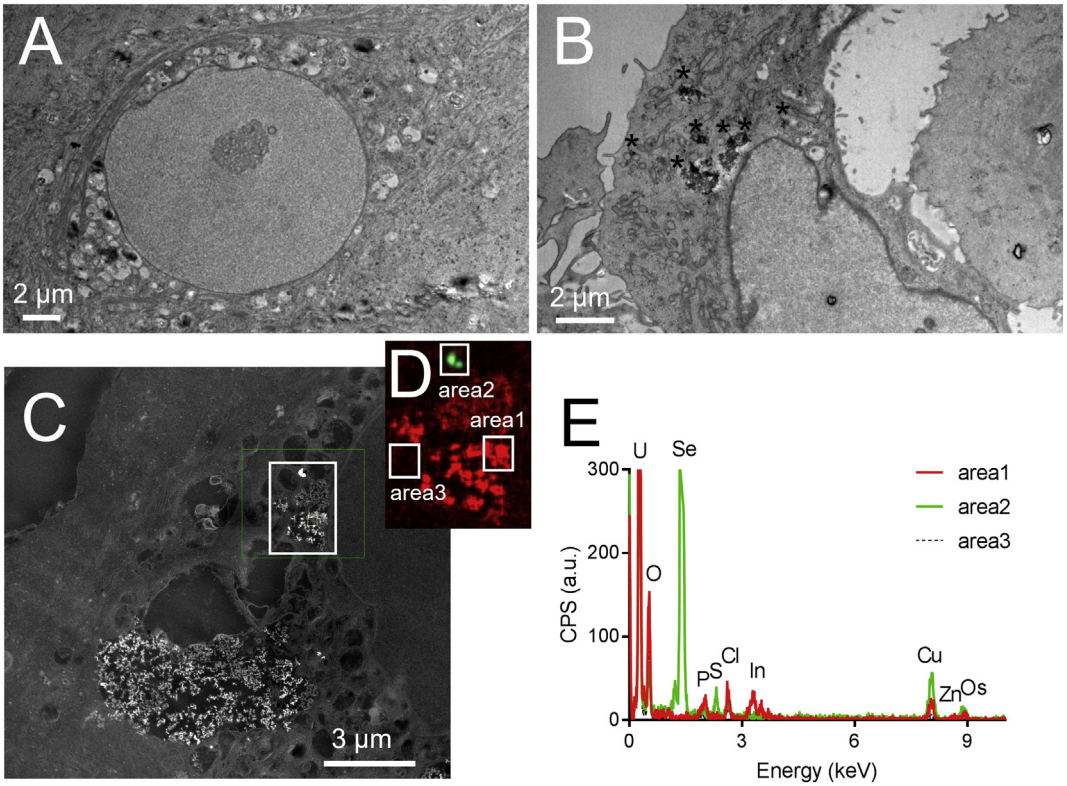

Fig. 8. TEM observation of keratinocytes exposed to InZnPS CS Pen QDs. Control cells (A) and cells exposed to aged InZnPS CS Pen (B, *: In-rich agglomerates). A region containing In-rich agglomerates was imaged using STEM, in HAADF mode (C), and analyzed via EDS. Reconstruction of In (red) and Se (green) chemical element distribution in the square highlighted in C (D). EDS spectra of the areas 1, 2 and 3 depicted in D (E).

Table 2
Results of the linear combination fits for the In K-edge EXAFS spectra[a].

		In species (molar %)				
	k range	In in pristine QD[a]	In acetate	In phosphate	Sum	R-factor[b]
QDs						
Aged InZnP CS Pen	2.4–12		52	44	96	0.06
Aged InZnPS CS Pen	2.4–12		53	44	97	0.05
Keratinocytes						
InZnP C GSH	2.4–12	21	42	31	94	0.08
InZnPS CS GSH	2.4–12	100			100	0.18
InZnPS C Pen	2.4–12	100			100	0.08
Aged InZnP CS Pen	2.4–12		53	37	90	0.09
Aged InZnP CS GSH	2.4–12		45	48	93	0.08
Aged InZnPS CS Pen	2.4–12		43	53	96	0.13
Aged InZnPS CS GSH	2.4–12		54	37	91	0.05

[a] For pristine QDs, InZnP and InZnPS were used for samples exposed to InZnP and InZnPS QD, respectively.
[b] Fit quality criterion provided by ATHENA (R factor = $\Sigma[k^2\,\chi_{exp} - k^2\,\chi_{fit}]^2/\Sigma[k^2\,\chi_{exp}]^2$.

studies, which were InP/ZnS QDs coated with mercaptopropionc acid (MPA) (Chibli et al., 2011; Soenen et al., 2014), while the QDs used in the present study are InZnP(S)/Zn(Se,S) QDs coated with Pen or GSH. Cytotoxicity studies reported here suggest that GSH (containing one thiol, one amino and two carboxy-groups) would provide better stabilization to QDs than Pen (containing one thiol, one amino and one carboxy-groups). MPA is even less complex than Pen, with only one thiol and one carboxy-group. One hypothesis would be that QDs used in the present studies are more stable, and therefore less toxic, than QDs functionalized with MPA. Moreover, for core-shell QDs, the presence of Se reduces the lattice mismatch between the core and the shell of these QDs, also enhancing their stability. Another hypothesis would be that primary human keratinocytes show better resistance to ROS, and more generally to QDs, than the cell lines used in these previous studies, for instance via a more active ROS scavenging activity. This would be in line with the different sensitivities towards QDs observed by Chibli et al. in different cell lines (Chibli et al., 2011).

5. Conclusion

In this study, a strong contrast was observed between the toxicity of pristine QDs, that were essentially non-toxic, and the toxicity of aged QDs, which proved to be all toxic. A key point turned out to be the secondary products created during the degradation, which showed a stronger toxic effect than pristine QDs. The presence of the Zn(Se,S) gradient shell efficiently protected the core of QDs from degradation, and therefore reduced their toxicity. Regarding core-only QDs, alloying the core with S facilitated transfer to aqueous solution due to the presence of a thin protective layer of ZnS. In this condition, QD cores were more stable when coated with GSH compared to Pen, therefore GSH ligand increased the safety of these QDs. This study highlights the importance of characterizing QD physico-chemical transformation under realistic lifecycle scenarios, i.e. long-term accelerated weathering in a climatic chamber, since it would have toxicological implications. The use of InP-based materials in the new generation of electronics makes it important to design safer InP compositions, anticipating secondary products which might be released in the environment upon degradation. Although this study was performed with primary human keratinocytes, which are the most relevant possible model of skin cells, it would be important to complement this study with data from in vivo experiments, since in vitro models do not reproduce the complexity of the skin. Finally, future studies should focus on the physicochemical transformation and effects of QDs contained in products that are already on the market. In these products, QDs are included in polymer matrices, which limit QD degradation and release of toxic substances, and therefore human and environmental exposure.

Acknowledgements

The authors thank ESRF and CRG committees for the provision of beamtime on FAME beamline (BM30B), and R. Soulas for imaging on TEM OSIRIS, supported and managed by Agence National de la Recherche (ANR), program ‘Investissements d'Avenir’, reference ANR-10-EQPX-39.

Funding

This work is a contribution to the Labex Serenade (ANR-11-LABX-0064) funded by the French Government's “Investissements d'Avenir” ANR program, through the A*MIDEX project (ANR-11-IDEX-0001-02). It was supported by the French National Research agency ANR (grant NEUTRINOS, ANR-16-CE09-0015-03), CNRS and Communauté Université Grenoble Alpes (ComUE, PEPS project SABYDE), and the French Environment and Energy Management Agency (ADEME). This work used the platforms of the Grenoble Instruct-ERIC Center (ISBG: UMS 3518 CNRS-CEA-UGA-EMBL) with support from FRISBI (ANR-10-INSB-05-02) and GRAL (ANR-10-LABX-49-01) within the Grenoble Partnership for Structural Biology (PSB). The electron microscope facility is supported by the Auvergne Rhône-Alpes Region, the Fondation Recherche Medicale (FRM), the fonds FEDER and the GIS-Infrastrutures en Biologie Sante et Agronomie (IBISA)

Declaration of competing interest

The authors declare no conflict of interest.

Appendix A. Supplementary data

Supplementary data to this article can be found online at https://doi.org/10.1016/j.impact.2019.100168.

References

Lin S, Yu T, Yu Z, Hu X, Yin D. Nanomaterials Safer-by-Design: An Environmental Safety Perspective. Advanced materials (Deerfield Beach, Fla). 2018;30(17):e1705691.
Alivisatos, A.P., 1996. Semiconductor clusters, nanocrystals, and quantum dots. Science 271 (5251), 933–937.
Armand, L., Tarantini, A., Beal, D., Biola-Clier, M., Bobyk, L., Sorieul, S., et al., 2016. Long-term exposure of A549 cells to titanium dioxide nanoparticles induces DNA damage and sensitizes cells towards genotoxic agents. Nanotoxicology 10 (7), 913–923.
Bastus, N.G., Puntes, V., 2018. Nanosafety: towards safer nanoparticles by design. Curr. Med. Chem. 25 (35), 4587–4601.
Beyersmann, D., Haase, H., 2001. Functions of zinc in signaling, proliferation and differentiation of mammalian cells. Biometals: an international journal on the role of metal ions in biology, biochemistry, and medicine 14 (3–4), 331–341.
Bharali, D.J., Lucey, D.W., Jayakumar, H., Pudavar, H.E., Prasad, P.N., 2005. Folate-receptor-mediated delivery of InP quantum dots for bioimaging using confocal and two-

photon microscopy. J. Am. Chem. Soc. 127 (32), 11364–11371.
Bomhard, E.M., 2016. The toxicology of indium tin oxide. Environ. Toxicol. Pharmacol. 45, 282–294.
Bottrill, M., Green, M., 2011. Some aspects of quantum dot toxicity. Chem. Commun. (Camb.) 47 (25), 7039–7050.
Brunetti, V., Chibli, H., Fiammengo, R., Galeone, A., Malvindi, M.A., Vecchio, G., et al., 2013. InP/ZnS as a safer alternative to CdSe/ZnS core/shell quantum dots: in vitro and in vivo toxicity assessment. Nanoscale 5 (1), 307–317.
Calabrese, G., Morgan, B., Riemer, J., 2017. Mitochondrial glutathione: regulation and functions. Antioxid. Redox Signal. 27 (15), 1162–1177.
Chibli, H., Carlini, L., Park, S., Dimitrijevic, N.M., Nadeau, J.L., 2011. Cytotoxicity of InP/ZnS quantum dots related to reactive oxygen species generation. Nanoscale 3 (6), 2552–2559.
Cho, D.Y., Xi, L., Boothroyd, C., Kardynal, B., Lam, Y.M., 2016. The role of ion exchange in the passivation of in(Zn)P nanocrystals with ZnS. Sci. Rep. 6, 22818.
Corazzari, I., Gilardino, A., Dalmazzo, S., Fubini, B., Lovisolo, D., 2013. Localization of CdSe/ZnS quantum dots in the lysosomal acidic compartment of cultured neurons and its impact on viability: potential role of ion release. Toxicology in vitro: an international journal published in association with BIBRA 27 (2), 752–759.
Derfus, A.M., Chan, W.C.W., Bhatia, S.N., 2004. Probing the cytotoxicity of semiconductor quantum dots. Nano Lett. 4 (1), 11–18.
Fitzpatrick, T.B., 1988. The validity and practicality of sun-reactive skin types I through VI. Arch. Dermatol. 124 (6), 869–871.
Gilbert, B., Huang, F., Zhang, H.Z., Waychunas, G.A., Banfield, J.F., 2004. Nanoparticles: strained and stiff. Science 305 (5684), 651–654.
Gwinn, W.M., Qu, W., Bousquet, R.W., Price, H., Shines, C.J., Taylor, G.J., et al., 2015. Macrophage solubilization and cytotoxicity of indium-containing particles as in vitro correlates to pulmonary toxicity in vivo. Toxicological sciences: an official journal of the Society of Toxicology 144 (1), 17–26.
Helle, M., Cassette, E., Bezdetnaya, L., Pons, T., Leroux, A., Plenat, F., et al., 2012. Visualisation of sentinel lymph node with indium-based near infrared emitting quantum dots in a murine metastatic breast cancer model. PLoS One 7 (8), e44433.
Huang, K., Demadrille, R., Silly, M.G., Sirotti, F., Reiss, P., Renault, O., 2010. Internal structure of InP/ZnS nanocrystals unraveled by high-resolution soft X-ray photoelectron spectroscopy. ACS Nano 4 (8), 4799–4805.
Huaux, F., De Gussem, V., Lebrun, A., Yakoub, Y., Palmai-Pallag, M., Ibouraadaten, S., et al., 2018. New interplay between interstitial and alveolar macrophages explains pulmonary alveolar proteinosis (PAP) induced by indium tin oxide particles. Arch. Toxicol. 92 (4), 1349–1361.
IARC, 1993. Cadmium and Cadmium Compounds. IRARC Monographs on the Evaluation of Carcinogenic Risks to Humans. 58. pp. 119–237.
IARC, 2006. Cobalt in hard metals and cobalt sulfate, gallium arsenide, indium phosphide and vanadium pentoxide. In: IRARC Monographs on the Evaluation of Carcinogenic Risks to Humans. 86. pp. 1–294.
Jarosz, M., Olbert, M., Wyszogrodzka, G., Mlyniec, K., Librowski, T., 2017. Antioxidant and anti-inflammatory effects of zinc. Zinc-dependent NF-kappa B signaling. Inflammopharmacology 25 (1), 11–24.
Kauffer, F.A., Merlin, C., Balan, L., Schneider, R., 2014. Incidence of the core composition on the stability, the ROS production and the toxicity of CdSe quantum dots. J. Hazard. Mater. 268, 246–255.
Kirchner, C., Liedl, T., Kudera, S., Pellegrino, T., Munoz Javier, A., Gaub, H.E., et al., 2005. Cytotoxicity of colloidal CdSe and CdSe/ZnS nanoparticles. Nano Lett. 5 (2), 331–338.
Kraegeloh, A., Suarez-Merino, B., Sluijters, T., Micheletti, C., 2018. Implementation of safe-by-Design for Nanomaterial Development and Safe Innovation: why we need a comprehensive approach. Nanomaterials (Basel, Switzerland) 8 (4).
Le Bars, M., Legros, S., Levard, C., Chaurand, P., Tella, M., Rovezzi, M., et al., 2018. Drastic change in zinc speciation during anaerobic digestion and composting: instability of nanosized zinc sulfide. Environ. Sci. Technol. 52 (22), 12987–12996.
Li, L., Reiss, P., 2008. One-pot synthesis of highly luminescent InP/ZnS nanocrystals without precursor injection. J. Am. Chem. Soc. 130 (35), 11588–11589.
Lim, J., Bae, W.K., Lee, D., Nam, M.K., Jung, J., Lee, C., et al., 2011. InP@ZnSeS, core@composition gradient Shell quantum dots with enhanced stability. Chem. Mater. 23 (20), 4459–4463.
Lin, R.H., Yang, M.L., Li, Y.C., Chang, H.M., Kuan, Y.H., 2013. Indium chloride-induced micronuclei via reactive oxygen species in Chinese hamster lung fibroblast V79 cells. Environ. Toxicol. 28 (10), 595–600.
Lin, G., Ouyang, Q., Hu, R., Ding, Z., Tian, J., Yin, F., et al., 2015. In vivo toxicity assessment of non-cadmium quantum dots in BALB/c mice. Nanomedicine: nanotechnology, biology, and medicine 11 (2), 341–350.
Litvin AP, Martynenko IV, Purcell-Milton F, Baranov AV, Fedorov AV, Gun'ko YK. Colloidal quantum dots for optoelectronics. J. Mater. Chem. A. 2017;5(26):13252–75.
Mancini, M.C., Kairdolf, B.A., Smith, A.M., Nie, S., 2008. Oxidative quenching and degradation of polymer-encapsulated quantum dots: new insights into the long-term fate and toxicity of nanocrystals in vivo. J. Am. Chem. Soc. 130 (33), 10836–10837.
Mattera, L., Bhuckory, S., Wegner, K.D., Qiu, X., Agnese, F., Lincheneau, C., et al., 2016. Compact quantum dot-antibody conjugates for FRET immunoassays with sub-nanomolar detection limits. Nanoscale 8 (21), 11275–11283.
Mouret, S., Baudouin, C., Charveron, M., Favier, A., Cadet, J., Douki, T., 2006. Cyclobutane pyrimidine dimers are predominant DNA lesions in whole human skin exposed to UVA radiation. Proc. Natl. Acad. Sci. U. S. A. 103 (37), 13765–13770.
Panfili, F.R., Manceau, A., Sarret, G., Spadini, L., Kirpichtchikova, T., Bert, V., et al., 2005. The effect of phytostabilization on Zn speciation in a dredged contaminated sediment using scanning electron microscopy, X-ray fluorescence, EXAFS spectroscopy, and principal components analysis. Geochim. Cosmochim. Acta 69 (9), 2265–2284.
Pons, T., Pic, E., Lequeux, N., Cassette, E., Bezdetnaya, L., Guillemin, F., et al., 2010. Cadmium-free CuInS2/ZnS quantum dots for sentinel lymph node imaging with reduced toxicity. ACS Nano 4 (5), 2531–2538.
Proux, O., Biquard, X., Lahera, E., Menthonnex, J.J., Prat, A., Ulrich, O., et al., 2005. FAME: a new beamline for X-ray absorption investigations of very-diluted systems of environmental, material and biological interests. Phys. Scr. T115, 970–973.
Proux, O., Nassif, V., Prat, A., Ulrich, O., Lahera, E., Biquard, X., et al., 2006. Feedback system of a liquid-nitrogen-cooled double-crystal monochromator: design and performances. J. Synchrotron Radiat. 13, 59–68.
Rahman, M.M., Hossain, K.F.B., Banik, S., Sikder, M.T., Akter, M., Bondad, S.E.C., et al., 2019. Selenium and zinc protections against metal-(loids)-induced toxicity and disease manifestations: a review. Ecotoxicol. Environ. Saf. 168, 146–163.
Ravel, B., Newville, M., 2005. ATHENA and ARTEMIS: interactive graphical data analysis using IFEFFIT. Phys. Scr. T115, 1007–1010.
Reiss, P., Carriere, M., Lincheneau, C., Vaure, L., Tamang, S., 2016. Synthesis of semiconductor nanocrystals, focusing on nontoxic and earth-abundant materials. Chem. Rev. 116 (18), 10731–10819.
Rocha, T.L., Mestre, N.C., Saboia-Morais, S.M., Bebianno, M.J., 2017. Environmental behaviour and ecotoxicity of quantum dots at various trophic levels: a review. Environ. Int. 98, 1–17.
Schwarz-Plaschg, C., Kallhoff, A., Eisenberger, I., 2017. Making nanomaterials safer by design? Nanoethics 11, 277–281.
Sharif, R., Thomas, P., Zalewski, P., Fenech, M., 2012. The role of zinc in genomic stability. Mutat. Res. 733 (1–2), 111–121.
Soenen, S.J., Manshian, B.B., Aubert, T., Himmelreich, U., Demeester, J., De Smedt, S.C., et al., 2014. Cytotoxicity of cadmium-free quantum dots and their use in cell bioimaging. Chem. Res. Toxicol. 27 (6), 1050–1059.
Sugiyama, K., Yu, J.H., Hiraga, K., Terasaki, O., 1999. Monoclinic InPO4 center dot 2H(2)O. Acta Crystallographica Section C-Crystal Structure Communications 55, 279–281.
Tamang, S., Lincheneau, C., Hermans, Y., Jeong, S., Reiss, P., 2016. Chemistry of InP nanocrystal syntheses. Chem. Mater. 28 (8), 2491–2506.
Thuy, U.T.D., Liem, N.Q., Thanh, D.X., Protiere, M., Reiss, P., 2007. Optical transitions in polarized CdSe, CdSe/ZnSe, and CdSe/CdS/ZnS quantum dots dispersed in various polar solvents. Appl. Phys. Lett. 91 (24).
Ung, T.D.T., Pham, T.T., Nguyen, Q.L., Li, L., Reiss, P., 2010. Comparative photoluminescence study of close-packed and colloidal InP/ZnS quantum dots. Appl. Phys. Lett. 96 (7), 3.
Vandebriel, R.J., De Jong, W.H., 2012. A review of mammalian toxicity of ZnO nanoparticles. Nanotechnol. Sci. Appl. 5, 61–71.
Wegner, K.D., Hildebrandt, N., 2015. Quantum dots: bright and versatile in vitro and in vivo fluorescence imaging biosensors. Chem. Soc. Rev. 44 (14), 4792–4834.
Wyckoff, R.W.G., 1963. Crystal Structure, Second edition. 1. New York Interscience Publishers, pp. 85–237.
Yaghini, E., Turner, H.D., Le Marois, A.M., Suhling, K., Naasani, I., MacRobert, A.J., 2016. In vivo biodistribution studies and ex vivo lymph node imaging using heavy metal-free quantum dots. Biomaterials 104, 182–191.
Yaghini, E., Turner, H., Pilling, A., Naasani, I., MacRobert, A.J., 2018. In vivo biodistribution and toxicology studies of cadmium-free indium-based quantum dot nanoparticles in a rat model. Nanomedicine: nanotechnology, biology, and medicine 14 (8), 2644–2655.